This is a repository copy of *Visualization of atomic scale reaction dynamics of supported nanocatalysts during oxidation and ammonia synthesis using in-situ environmental (scanning) transmission electron microscopy*.

White Rose Research Online URL for this paper:
https://eprints.whiterose.ac.uk/167570/

Version: Accepted Version

Journal Pre-proofs

In-situ visualization of atomic scale reaction dynamics of supported nanocatalysts during oxidation and ammonia synthesis using environmental (scanning) transmission electron microscopy

Michael R. Ward, Robert W. Mitchell, Edward D. Boyes, Pratibha L. Gai

We dedicate this article to the memory of Professor Dangsheng Su, a great colleague and a distinguished scientist.

In-situ visualization of atomic scale reaction dynamics of supported nanocatalysts during oxidation and ammonia synthesis using environmental (scanning) transmission electron microscopy

Michael R. Ward [a,b], Robert W. Mitchell [a,b], Edward D. Boyes [a,b,c,*], Pratibha L. Gai [a,b,d,*]

[a] *The York Nanocentre, University of York, York YO10 5DD, UK*

[b] *Department of Physics, University of York, York YO10 5DD, UK*

[c] *Department of Electronic Engineering, University of York, York YO10 5DD, UK*

[d] *Department of Chemistry, University of York, York YO10 5DD, UK*

[*] **Corresponding authors.**

Email addresses: pratibha.gai@york.ac.uk (P.L. Gai); ed.boyes@york.ac.uk (E.D. Boyes)

Abstract

Reaction dynamics in gases at operating temperatures at the atomic level are the basis of heterogeneous gas-solid catalyst reactions and are crucial to the catalyst function. Supported noble metal nanocatalysts such as platinum are of interest in fuel cells and as diesel oxidation catalysts for pollution control, and practical ruthenium nanocatalysts are explored for ammonia synthesis. Graphite and graphitic carbons are of interest as supports for nanocatalysts. Despite considerable literature on the catalytic processes on graphite and graphitic supports, reaction dynamics of the nanocatalysts on the supports in different reactive gas environments and operating temperatures at the single atom level are not well understood. Here we present real time in-situ observations and analyses of reaction dynamics of Pt in oxidation, and practical Ru nanocatalysts in ammonia synthesis, on graphite and related supports under controlled reaction environments using a novel environmental (scanning) transmission electron microscope with single atom resolution. By recording snapshots of the reaction dynamics, the behaviour of the catalysts is imaged. The images reveal single metal atoms, clusters of a few atoms on the graphitic supports and the support function. These all play key roles in the mobility, sintering and growth of the catalysts. The experimental findings provide new structural insights into reaction dynamics, morphology and stability of the nanocatalysts.

Keywords:

1. Introduction

Heterogeneous catalysis plays a major role in the development of chemical technology [1–3]. Many heterogeneous reactions involve gas-solid catalyst (or liquid-solid catalyst-gas) reactions enabling the production of energy, food, chemicals and a cleaner environment [1-8]. The reactions take place at the atomic level and structural changes form under dynamic reactive gas environments and operating temperatures. The development of the atomic resolution environmental transmission electron microscope (atomic resolution-ETEM) [4], which is advanced with single atom resolution [5], enable the visualization and analysis of gas-solid catalyst reactions under controlled environments in real time at the atomic level. The design and development of a windowless-liquid TEM holder to visualize low vapour pressure liquid-solid catalyst reactions in gas environments at operating temperatures at the sub-nanometer level has been reported [6], with applications in novel hydrogenation chemistry to produce chemicals and polymers [7].

In heterogeneous and electrochemical catalysis, carbon materials including graphite are of interest as supports for precious metals [1,2]. Supported platinum nanoparticles are catalytically active in a variety of applications, including fuel cells to meet energy demands [1,2] and diesel oxidation catalysts [8], as well as in many industrial processes. The size and shape of the metal nanoparticles, their dispersion, stability on the support, nanoparticle-support interactions and the nature of the support (which can affect electronic properties of the nanoparticles) are known to influence their performance in reactions [1–3,8,9]. In fuel cell applications graphite is of increasing interest as a potential durable support to overcome corrosion issues of other carbon supports [1,10]. Platinum is an expensive metal and therefore atomic structural insights into mobility and dispersion of Pt under reactive environments are required to help optimise the stability and metal content.

Many heterogeneous chemical processes employ supported nanoparticle catalysts which often function at elevated temperatures. This can cause nanoparticles to migrate and

coalesce, or undergo Ostwald Ripening whereby atoms from less stable structures diffuse across the support and are stabilised on larger structures [11], leading to sintering. Particle sintering (coarsening) and growth leads to the loss of surface area, loss of stability and the loss of performance of the nanoparticle catalysts. The resulting large particles, where most of the precious metal is locked away beneath the surface, are unable to engage properly in catalytic processes [12].

To reduce the amount of costly precious metal required, atomically dispersed catalysts are being explored where dominant active sites are believed to be single atoms and/or small atom clusters. Single atom species and small atom clusters are especially of interest for catalysis applications, since they can potentially lead to more active sites to bind reagents [3,13–15]. Simulations and shape selective synthesis of supported platinum nanoparticles have shown the influence of the particle shape on the reactivity of the nanoparticles [9,16,17]. In supported Pt nanocatalyst systems, the support material for platinum nanoparticles (NPs), atoms and clusters, has often been an oxide [8,13], but different forms of carbon such as graphene, nanotubes and graphite are also being explored in heterogeneous and electrochemical catalysis [1,10] . Because of their high surface area and electronic properties, graphite supported Pt nanoparticle catalyst systems are of interest in fuel cells and as DOCs [1,2,10]. Structures of supported nanoparticles have been investigated using conventional TEM and STEM, in high vacuum and at room temperature, and with in-situ TEM [13–17,18]. As is well established, in STEM-high angle annular dark field (HAADF) imaging the image intensity is approximately proportional to Z^2 where Z is the atomic number [19]. There are reports on the advantage of STEM-HAADF imaging over TEM, including for accurate measurements of particle size distributions (PSD) performed at the nanometer (nm) level [20]. In STEM-HAADF, atoms on supports are much more readily discernible [19] than by

other methods. Aberration correction (AC) to correct electron lens aberrations [21] and methods to identify single atoms [22] have been reported in the literature.

As structural changes can often only exist under reaction environments, observations under controlled reaction conditions are required to obtain insights into reaction dynamics, which are crucial for the production and stabilization of nanocatalysts. To visualize and analyze gas-solid catalyst chemical reactions in real time under controlled reaction conditions at the single atom level, we have developed a novel double aberration corrected environmental (scanning) transmission electron microscope (referred to as E(S)TEM) with single atom resolution [5,23–26], which is described in the Experimental section. The atomic resolution-E(S)TEM has both ESTEM and ETEM capabilities [23–26].

In this research, we present in-situ ESTEM studies at single atom resolution to directly observe and analyze how platinum disperses and sinters on graphite surfaces in oxygen gas environments at operating temperatures between 200 °C and 700 °C, and the effect of the graphite support on the size, morphology and the stability of the particles. To our knowledge, dynamic ESTEM studies of the oxidation of Pt/graphite at single atom resolution have not been reported previously in the literature.

Additionally, reaction dynamics of other nanometals on graphitic carbon in different gas environments and temperatures are explored using the E(S)TEM at single atom resolution. We describe observations of dynamic ammonia synthesis over practical ruthenium (Ru) nanocatalysts supported on graphitic carbon and compare the findings to those on amorphous carbon supports. Graphitic carbon is an important support for precious metals like Ru in ammonia synthesis. Ammonia is a key chemical for the production of fertilizers for food production, polymers and in chemical synthesis [27–33]. In heterogeneous catalysis for ammonia synthesis solid state catalysts are employed to improve the rate of formation of

ammonia from the diatomic gas precursors, nitrogen and hydrogen, in the reaction: N_2+3H_2 → $2NH_3$. Historically, the industrial catalyst most widely used for the synthesis process is the Haber catalyst based on promoted iron oxides supported on ceramic oxide supports such as alumina [27]. More recently, alternative graphitic carbon supported ruthenium catalysts have been explored which can operate more efficiently and at lower pressures than the iron catalysts [28,32]. Earlier literature reports of supported Ru systems have focused primarily only Ru particles and the catalyst performance is suggested to be influenced by Ru particles with sizes of up to several nanometers (nm) [31,33]. Therefore, atomic scale reaction dynamics and stability of the nanoparticle catalysts in the presence of atomic species during ammonia synthesis as a function of temperature and time, are not well understood. An improved understanding of the atomic scale dynamics between the gas and the nanocatalysts in their functioning state under controlled ammonia synthesis environments is therefore required. The insights would be important in controlling and optimizing the dispersion and stability of the nanocatalysts for their applications.

Here, we have carried out real time in-situ studies of dynamic ammonia synthesis on supported practical ruthenium nanoparticle catalysts prepared by chemical methods relevant to industrial processes. The dynamics of Ru nanocatalysts on different carbon supports under simulated ammonia synthesis reaction conditions have been probed at the single atom level using the E(S)TEM to obtain a deeper understanding of interactions between the gas and the nancatalysts during ammonia synthesis. Observations of reacting single atoms and clusters of atoms in practical samples on uneven supports and among the much larger nanoparticles can be challenging, but this can be addressed using the ESTEM.

2. Experimental

2.1. Sample preparation

2.1.1. Pt/graphite nanoparticle systems

A MEMS (micro-electromechanical system) heating holder from DENSsolutions was employed with Si_3N_4 film window MEMS chips. The Si_3N_4 (hereinafter referred to as SiN_x) was approximately 20 nm thick. The SiN_x also acts as a stable support for catalyst powders. Graphite flakes (Strem Chemicals) were deposited on the MEMS chips via ethanol suspension. The dispersion was treated in an ultrasonic bath for 5 min and deposited on the MEMS chips using a pipette. Platinum was deposited directly on the MEMS chips on areas containing graphite, and on regions with only SiN_x, using a JEOL 2300HR sputter deposition machine using a 99.99 % pure platinum target. A nominal thickness of 0.2 nm was chosen to provide a dispersion consisting of isolated atoms, clusters of a few atoms and some nanoparticles, as used before [23]. 0.2 nm was the minimal setting which could be readily reproduced. Comparison with oxidation dynamics of Pt on amorphous carbon support at high temperatures was not possible as the sample was observed to disintegrate at temperatures above 300 °C in oxygen gas. Therefore, a more stable support SiN_x was employed for the comparison.

2.1.2. Graphitic carbon and carbon supported practical Ru nanocatalysts

For E(S)TEM studies ruthenium on graphitic carbon (here after referred to as: **Ru/*g*-C)** samples were prepared as follows: Ru (from a few wt% up to 20 wt%) was loaded onto graphitic carbon supports via incipient wetness impregnation method using aqueous $Ru(NO)(NO_3)_3$, (ruthenium nitrosyl nitrate) and subsequently dried in air at 150 °C for 12 h. The samples were deposited onto 5 nm amorphous carbon coated MEMS chips purchased from DENS solutions.

For comparison ruthenium on amorphous carbon (**Ru/*am*-C**) samples were also prepared. Aqueous Ru $(NO)(NO_3)_3$ (2 μL, 2 mg/mL) was deposited directly onto an amorphous carbon MEMS chip and dried in air at 150 °C for 2 h.

2.2. ESTEM experiments

Boyes and Gai [4] pioneered the design, construction and development of the atomic resolution-environmental transmission electron microscope (atomic resolution-ETEM) to visualize and analyze gas-solid (catalyst) reactions under controlled reaction conditions in real-time at the atomic level, with applications to catalysis [34–38]. The ETEM [4] is used by EM manufacturers and in laboratories globally [3,37]. In the ETEM, gas pressures of a few mbars are normally used for atomic resolution studies and gas pressures of many mbars are possible [4,34–37]. We have now advanced the ETEM and designed and constructed a double aberration corrected (AC) E(S)TEM by modifying the JEOL 2200FS AC (S)TEM [5,23–26]. The novel instrument supports both the full ESTEM and ETEM functionalities [23–26,39–45], with differentially pumped column sections, and is shown in the schematic in Fig. 1. The instrument enables the visualization and analysis of gas-solid (catalyst) reactions in real time, at the single atom level. In the ESTEM, single atom resolved HAADF imaging and full analytical functionalities including dynamic electron diffraction, energy dispersive X-ray spectroscopy (EDX) and electron energy loss spectroscopy (EELS), are enabled for the first time under controlled chemical reaction conditions of high temperatures in a continuously flowing gas atmosphere around the samples [23–26] . Gas pressures of 1–20 Pa cover sample surfaces, with many thousands of monolayers of gas per second covering the sample surface at the 1 Pa used for ESTEM. This is fully adequate to flood the surface of the EM sample with gas molecules and to drive the chemistry [23–26,41–43]. These are under conditions defined in surface science as 'high pressure' [46].

7
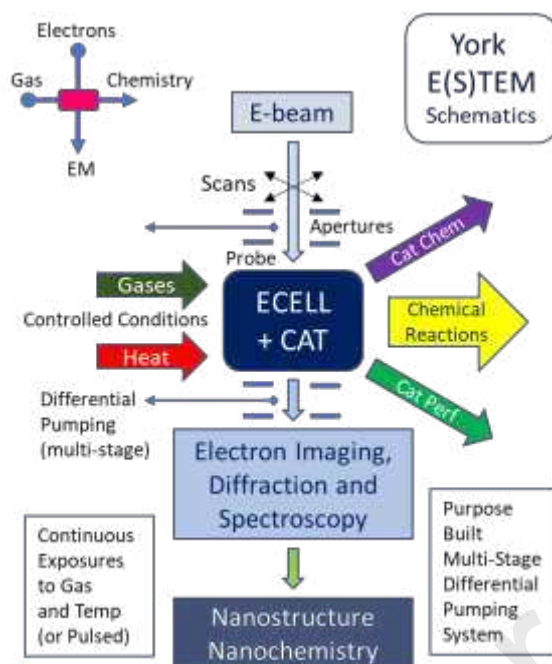
Fig. 1. A schematic of the imaging and chemical reaction in the instrument. CAT=catalyst, ECELL=environmental (reactor) cell.

In the dynamic in-situ experiments presented here, careful calibration procedures were employed to avoid deleterious effects of the electron beam on the reactions. Blank in-situ calibration experiments were carried out by beam blanking. The beam was blanked during reaction experiments to minimize the sample exposure to the beam and the particles were only exposed to the beam during data setup, interval examinations and actual data acquisition [3,23–26,39–41]. This approach has been simplified by the positional stability of the MEMS stages over extended periods of time. The data were cross-checked with in-situ experiments under the same reaction conditions using low dose electron beam currents [40]. Single atoms were identified using the established procedures [22] and by calibration and nornmalization of ESTEM-HAADF intensities [23].

For ESTEM studies we used image magnifications between 1.2 million (M) and 12 M. Images were recorded with 1024×1024 line frames with pixel dwell times of 19.5 µs. The

collection angles for HAADF imaging were 110 mrads and 170 mrads for the inner and outer

diameter of the detector, respectively.

3. Results and discussion

3.1. Pt/graphite

Fig. 2 shows characterization of the Pt/graphite sample. SiNx support (indicated at S)

and regions with graphite flakes (G) on a MEMS chip are shown in the TEM image in Fig.

2(a), with the corresponding electron diffraction (ED) patterns inset for SiN_x and graphite.

ED pattern of the graphite sheets indicates, as is to be expected, that it is close to the [001]

zone axis. Fig. 2(b) illustrates STEM-HAADF images of Pt nanoparticles on the S and G

supports.
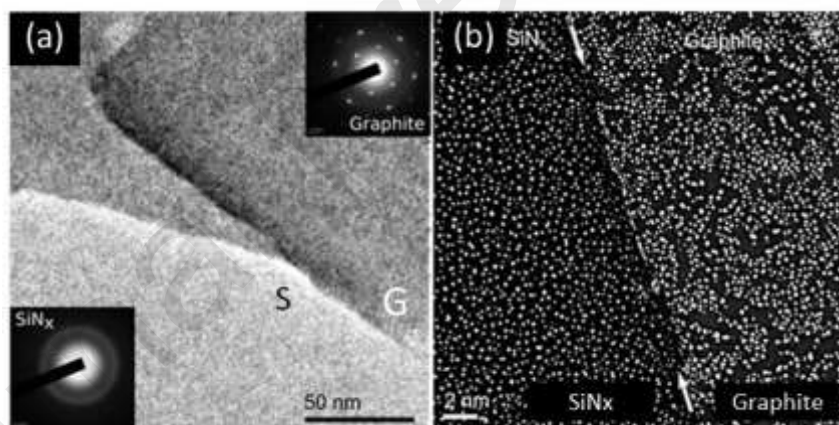
Fig. 2. (a) Graphite flakes (indicated by G) on Si_3N_4 (or SiN_x) MEMS chip (indicated by S) with inset electron diffraction patterns for SiN_x and that for graphite. (b) STEM-HAADF image at much higher magnification of platinum particles on SiN_x (S) and graphite regions (G) on a MEMS chip.

To minimize any initial contamination, the sample was heated from room temperature

(RT) to 300 °C in vacuum for about 10 sec. It was then heated at 500 °C in vacuum for 30

min to achieve the formation of more regularly shaped particles, instead of irregular raft

9

structures frequently found on sputtered films, and with a view to remove any contamination. The sample after this heating process was selected as the starting reference point.

Fig. 3 (a and b) are ESTEM-HAADF images showing the presence of individual Pt atoms (revealed as white dots [23]), atom clusters and nanoparticles of Pt in the as deposited platinum on SiN$_x$ and graphite regions, respectively, recorded at RT, after heating at 500 ℃ for 30 min in vacuum. In Fig. 3(c) the presence of individual Pt atoms shown in the inset (about 0.1 nm in size indicated by arrows) is identified by the intensity profile and measuring the FWHM. This post-heated sample is used as a reference point. In general, the platinum structures on both supports are primarily disordered Pt atom clusters and Pt single atoms, but there is a greater fraction of ordered crystals on the graphite; revealing 0.23 nm lattice spacing of Pt (111). The atomic structure of the graphite cannot be directly be directly resolved on the SiN$_x$ due to the strong ESTEM-HAADF image signal from the SiN$_x$ support. In BF-STEM images however the atomic planes are found to be visible.
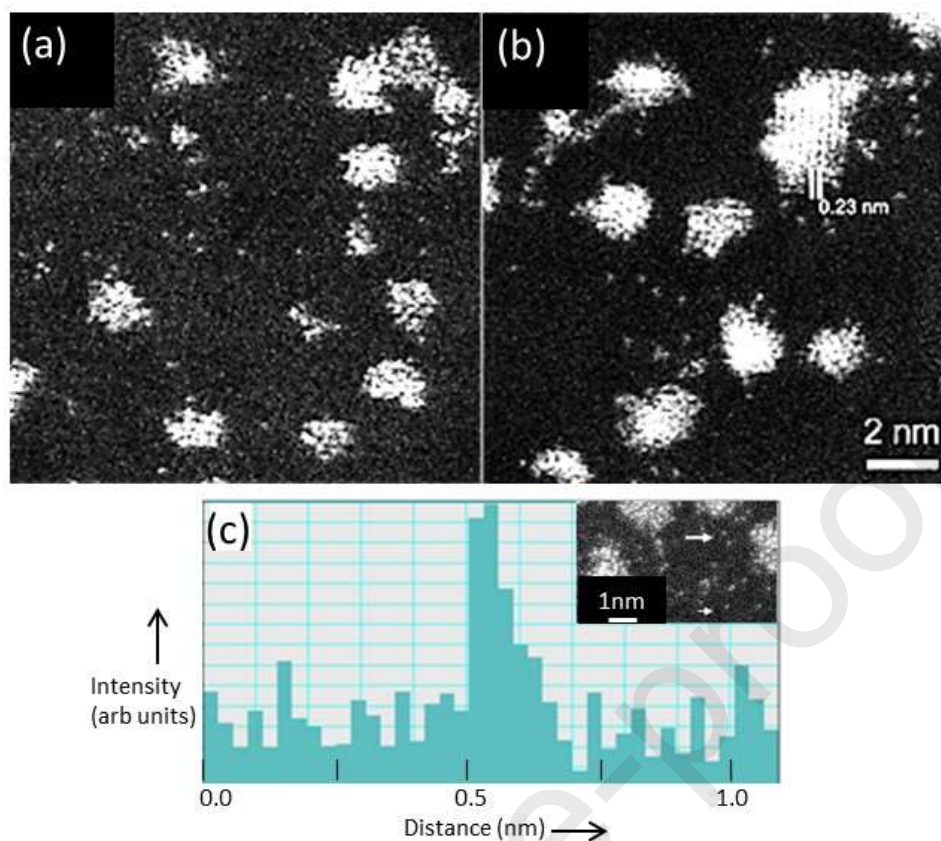
Fig. 3. ESTEM-HAADF images of the platinum single atoms, Pt atom clusters and irregular Pt nanoparticles following heating at 500 °C for 30 min on: (a) Si_3N_4 (SiN_x) and (b) graphite regions. Pt lattice with 0.23 nm spacings are visible. (c) The presence of individual Pt atoms shown in the inset (about 0.1 nm in size indicated by arrows) is identified by the intensity profile.

Although the nanoparticle sizes are similar between the two regions, the concentration of nanoparticles is observed to be slightly higher on the graphite regions. It is believed that Pt (and other metals) does not adhere well to clean graphite surfaces [1,10] and those that do tend to form bonds with layers of contamination. Low energy facets such as {111} and {100} were observed, with a few {110} facets. However, the shapes of many particles were largely irregular.

3.2. Oxidation reactions

The post-heated sample was taken as the starting reference point. We carried out detailed studies of oxidation at different operating temperatures, as a function of time. Oxygen gas was injected on the starting reference samples (after the initial formation of the particles shown in Fig. 4(a) and the temperature was increased in 50 °C steps every minute until the desired temperatures of 200 °C, 350 °C, 500 °C and 700 °C were reached. A temperature of about 650 °C is known to encourage Ostwald ripening [11]. Reactions of the nanoparticles in oxygen gas at 200 °C for 6 h resulted in minor changes on the SiN_x regions (with average particle sizes of 1.57 nm) and larger particles on graphite (1.89 nm), illustrated in histogram analyses of the dynamic experimental observations shown in Fig. 4(b). The structures on the post-reacted sample were generally raft-like structures.
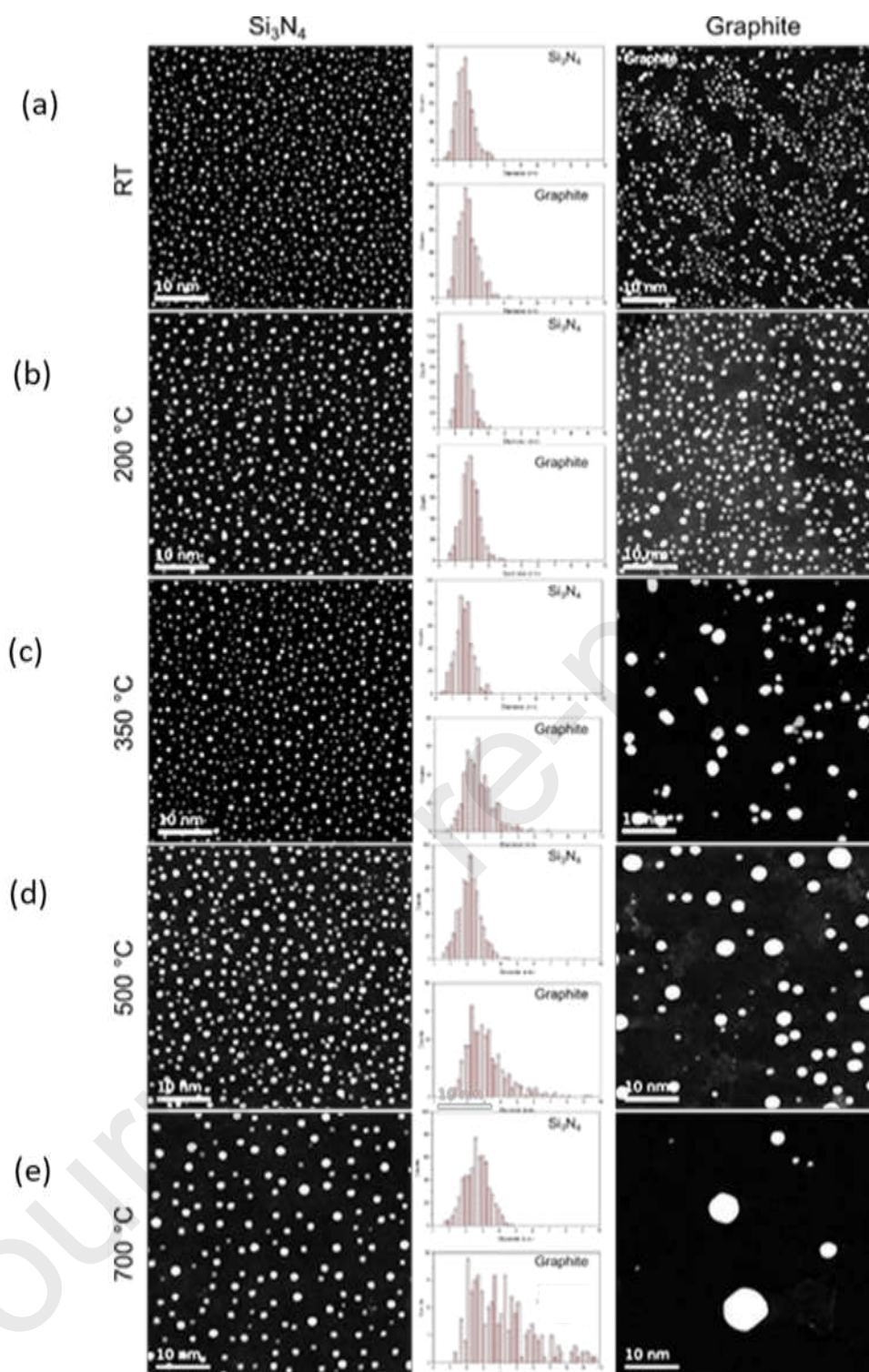
Fig. 4. Real time in-situ dynamic ESTEM-HAADF images in oxygen gas environments at operating temperatures. The initial reference image (a) is taken at RT following heating at 500 °C in vacuum**;** (b) dynamic reaction in oxygen at 200 °C for 6 hours; and (c–e) dynamic oxidation after 6 hours at 350 °C, 500 °C and 700 °C, respectively. (Scale bar is 10 nm).

After the reaction at 350 °C for 6 h in oxygen gas, a significant change in the nanoparticle dispersion was observed on the graphite regions. There is a clear increase in the number of particles over 3 nm in diameter, indicating that most nanoparticles on the graphite are highly mobile, compared to those on the SiN_x substrate. The particle dispersion on SiN_x regions at 350 °C for 6 h in oxygen gas was almost identical to that in the reference sample (Fig. 4a). The particle dispersion on the graphite in oxidation reactions was not uniform, with discrete regions of small and large nanoparticles with different shapes and increased faceting, particularly near the graphite edges (Fig. 4c).

It is reported that contaminants and more stable oxide species at graphite edges could stabilize the platinum [1,2]. In the plan view shown in ESTEM images of the reaction dynamics, the electron beam must transit through the Pt particles then the interface region and finally the support. EELS method to establish the nature of the Pt-graphite interface and the graphite edges is difficult to access, especially with our current holder equipment. This method works best for light elements with low energy losses. Pt on the other hand, is a heavy metal with a complex edge shape with relatively low contrast against the background. The challenge is to detect subtle changes that may be present on strong main component signals, which is difficult in the complex Pt nanocatalysts.

Oxidation at 500 °C for 6 h yielded a similar effect compared to that at 350 °C on the graphite regions except the nanoparticles were slightly larger with more faceted shapes. In-situ observations of the oxidation at 700 °C for 6 h showed many large faceted nanoparticles. The mean nanoparticle sizes from the oxidation experiments are summarized in Table 1.

Table 1 – Summary of nanoparticle sizes for the fresh and oxygen reacted catalysts

Sample	Mean (nm)	Std. Dev. (nm)
SiN$_x$ reference sample	1.67	0.51
SiN$_x$ 200 °C Oxygen gas	1.57	0.42
SiN$_x$ 350 °C Oxygen gas	1.67	0.51
SiN$_x$ 500 °C Oxygen gas	2.15	0.63
SiN$_x$ 700 °C Oxygen gas	2.65	0.72
Graphite reference sample	1.82	0.58
Graphite 200 °C Oxygen gas	1.89	0.51
Graphite 350 °C Oxygen gas	2.62	0.81
Graphite 500 °C Oxygen gas	3.15	1.21
Graphite 700 °C Oxygen gas	4.79	3.25

The findings reveal that at the higher temperatures of 350 °C and 500 °C Pt particles are larger on graphite in oxidation reactions indicating that Pt is much more mobile on that support. On the SiN$_x$ there are more significant metal-support interactions and particle coarsening is much more limited. The data provide insights into the reaction dynamics, dispersion and stability of Pt on graphite in the controlled oxidation process as a function of temperature. The larger particles also exhibited better crystallinity with Pt being the predominant chemical state.

The change in particle shapes and growth of nanoparticles observed on graphitic supports can be explained as following. The interrelated performance and stability of supported metal nanoparticle catalysts is influenced by weak or strong metal-support interactions in reactive gas environments at operating temperatures. Typically, both the amount and nature of active surfaces is diminished over time on stream, and the consequent particle size coarsening. Coarsening can involve both or either of metal atom diffusion between particles (leading to Ostwald ripening processes), or particle mobility, coalescence and sintering. Either way the material diffuses across the support surface and sometimes into it. The observations of Pt particle coarsening on graphite as a function of temperature have revealed that coarsening becomes significant at higher temperatures, leading to the loss of surface area and deactivation. They indicate that the particles are more mobile on the

15

graphite support with relatively weak interactions with the support. We believe that in addition to particle surface energy effects with sintering and morphology changes at higher temperatures, the minimization of interfacial energy between the metal nanoparticle and the support, and the resulting change in the nature of the contact between them, contribute to the increased migration of the particles.

3.3. Practical Ru nanocatalysts on graphitic carbon and carbon supports for ammonia synthesis: E(S)TEM analysis with single atom resolution

We studied reaction dynamics of the supported Ru nanocatalysts using ESTEM and ETEM under controlled environments as a function of temperature in hydrogen and nitrogen gas mixtures for ammonia synthesis. The supported Ru samples were subjected to initial reduction in hydrogen in-situ in the E(S)TEM to remove any oxide layers and form Ru particles, using reported procedures [27,29]. The hydrogen reduction was performed at ~ 400 °C for about 4 h. The sample was cooled to room temperature (RT) and the EM reaction chamber was outgassed before introducing $3H_2 + N_2$ gas mixture for ammonia synthesis. The hydrogen-reduced samples are hereafter referred to as post- reduction samples. High-purity hydrogen and nitrogen gases (99.9995% from BOC UK) were used in the in-situ experiments for both the preliminary hydrogen reduction and ammonia synthesis.

Suitable sample regions were identified in the ESTEM experiments. The samples were reacted in a H_2 and N_2 gas mixture with a 3:1 ratio at 1 Pa for ammonia synthesis. Dynamic images were recorded to examine the reaction dynamics, dispersion and stability of Ru clusters, Ru single atoms and Ru nanoparticles, as well as particle sintering.

In the in-situ ETEM studies of Ru/am-C, Ru nanoparticles were observed following the reduction at 450 °C for 1 h in H_2 gas shown in Fig. 5(a). In addition to <1 nm clusters, a majority of the Ru particles were in the size range of about 1 nm and up to about 2.5 nm, with

many faceted particles and a few larger particles. The observed lattice image spacings of the particles were consistent with the P63/mmc Ru phase. The nanoparticles were predominantly in (100), (002) and (200) crystal orientations. Fig. 5(b and c) show reaction dynamics of Ru nanoparticles on carbon in 3:1 H_2/N_2 gas mixture for ammonia synthesis at 300 °C for 2 h and 450 °C for 1 h, respectively. Migration and coalescence of Ru particle are observed following the treatments at both 300 °C for 2 h and 450 °C for 1 h during the synthesis. The larger particles in the latter are about 3nm. The observations in the synthesis reveal that larger Ru nanoparticles are well faceted and that small Ru particles are retained after the reaction. An area near the arrow from Fig. 5(b) is enlarged in Fig. 5(d), illustrating the formation of well-faceted nanoparticles. The increased faceting may be due to the minimization of the surface energy of particles as reported in the literature [23]. However, the presence of single atoms was not clearly discernible in the ETEM images due to diffraction and phase effects [25], and therefore the ESTEM was employed, which is described in the following sections. Chemical composition map using energy dispersive spectroscopy (EDX) of the initial sample shows an overall distribution of Ru across the sample, which is shown in Fig. 5(e).
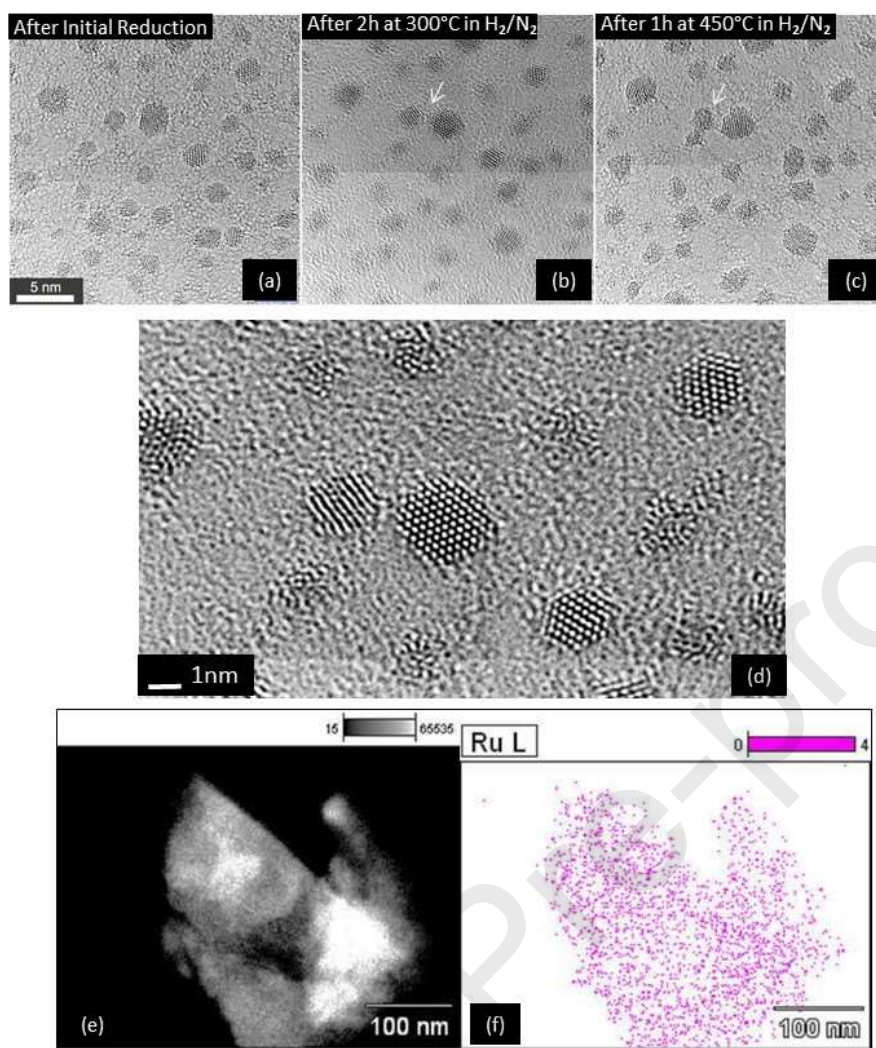
Fig. 5. Real time in-situ observations of reaction dynamics of Ru/am C (from the same area of the sample) in ammonia synthesis using atomic resolution-ETEM: (a) shows Ru nanoparticles observed in reduction at 450 °C for 1h in H_2 gas. The larger particles are well faceted. (b and c) show Ru nanoparticles on carbon in 3:1 H_2/N_2 gas mixture for ammonia synthesis at 300 °C for 2 h and 450 °C for 1 h, respectively. Coalescence of some Ru particles is observed at the higher temperature (e.g. indicated by a white arrow). The scale bar is 5nm. (d) An enlarged area from (b) indicating well-faceted Ru nanoparticles, with the large faceted particle of about 2.5 nm. (e) Composition map (EDX) of the initial sample shows a uniform overall distribution of Ru across the sample.

The ESTEM observations reveal the presence of a large number of Ru single atoms, clusters of Ru atoms (not visible in Fig. 5) and Ru nanoparticles on the support in the 3:1 H_2/N_2 gas mixture in the Ru/am C sample, which are shown in Fig. 6(a). To our knowledge images of Ru single atoms and clusters of Ru atoms in carbon supported practical Ru nanocatalysts in ammonia synthesis have not been reported previously. The inset shows the intensity profile of a small atom cluster in the white rectangle box marked 'a-b', which is enlarged in Fig. 6(b). Ru atoms and clusters are of crucial importance in understanding the dispersion and the stability of Ru in the synthesis.
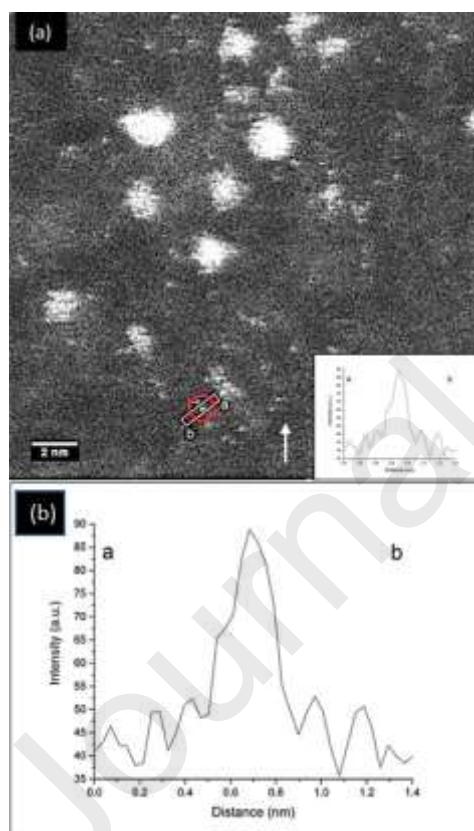
Fig. 6. A representative area in practical Ru/am C sample in $3H_2$ and N_2 gas mixture, revealing the presence of a large number of Ru single atoms and clusters of a few Ru atoms (e.g. indicated near the arrow), as well as Ru nanoparticles on the support. Single atoms measure about 0.1 nm. The inset shows the intensity profile of a small atom cluster in the white rectangle box marked 'a-b'. The scale marker is 2 nm. The inset is enlarged in (b).

In-situ ESTEM-HAADF observations of the reaction dynamics of a practical Ru/C nanocatalyst in ammonia synthesis as a function of temperature and time are shown in Fig. 7.
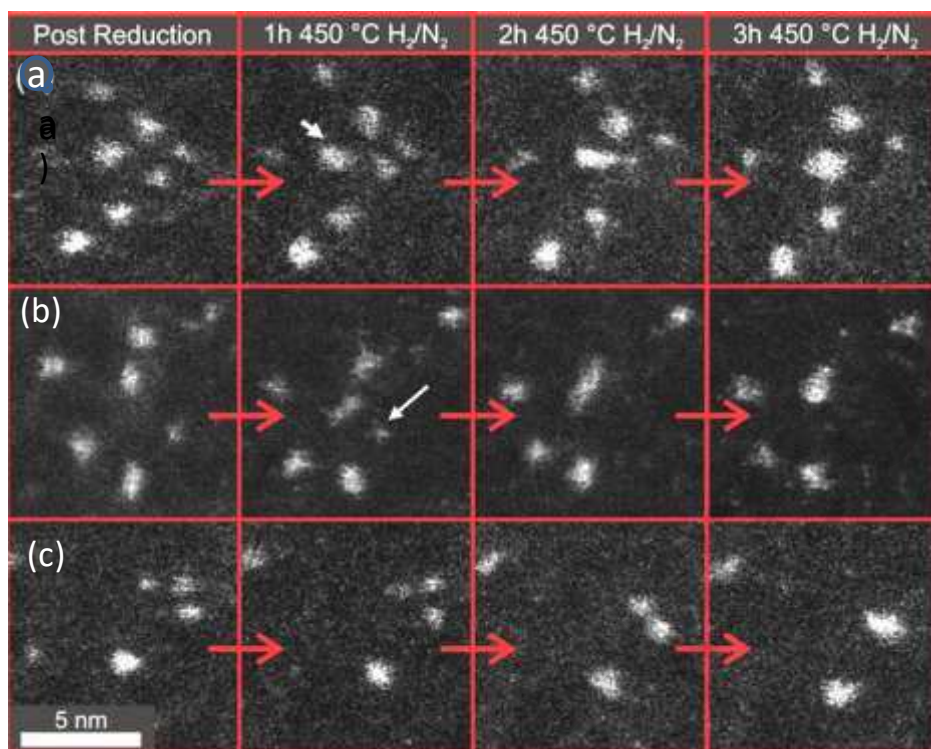
Fig. 7. Real time in-situ ESTEM-HAADF image sequence recorded showing reaction dynamics of practical Ru/C nanocatalyst in ammonia synthesis as a function of temperature and time. The figure shows dynamic images recorded in ammonia synthesis from 3 areas of the sample containing Ru clusters and nanoparticles (top row, middle row and bottom row). From left to right (from the same sample area) are: (a) top row: (1) post-hydrogen reduced sample showing Ru clusters and small NPs; (2) at 450 °C for 1h during ammonia synthesis (N_2+3H_2 mixture); (3) at 450 °C for 2h during ammonia synthesis; (4) at 450 °C for 3h during ammonia synthesis. Similarly, middle row (b) and bottom row (c) show reaction dynamics at these temperatures and time scales. Decay of small Ru cluster (e.g. indicated by a white arrow in the second image of the middle row) is observed (the 3rd mage in the middle row). At the longer time-scales coalescence of some nanoparticles is also observed.

The observations at higher temperatures and time reveal that irregular nanoparticles are replaced by more faceted particles. The findings are consistent with reports of enhanced faceting in supported nanoparticles under reduction reaction conditions [23].

Dynamic ETEM image sequence and corresponding dynamic electron diffraction patterns in ammonia synthesis using the $3H_2$ and N_2 gas mixture is presented in Fig. 8 for the Ru/g-C sample with 20wt% Ru. The uniformly distributed Ru nanoparticles are observed to be primarily disordered, irregular shaped particles with sizes ranging from 0.5 nm of about 1 nm. Fig. 8(a and c) show the image of Ru particles and the corresponding ED patterns in the gas mixture at RT (after the initial hydrogen reduction, referred to as post-reduced sample). The observations of the complex nanostructure following ammonia synthesis at 450 °C for 2 h revealed increased ordering and crystallinity (Fig. 8b), also evidenced by the corresponding dynamic ED (shown in Fig. 8d). In addition, the growth of Ru particles on the graphitic carbon support was observed with sizes between 1.6 and 2.5 nm, with some particles growing to sizes of about 5 to 7 nm. The growth is illustrated in Fig. 8(e). The dynamic observations in ammonia synthesis also reveal that the morphology of the nanoparticles on graphitic carbon is different to that on the amorphous carbon support, with less-faceted nanoparticles (i.e. with irregular or disordered surfaces) and some much larger particles, compared to those on the amorphous carbon support. The observations of the larger particle growth on the graphitic carbon (with the particle sizes between 5 and 7nm) indicate that the clusters and particles are more mobile on this support, with relatively weak metal-support interactions. Irregular Ru nanoparticles are replaced by the faceted particles in the Ru/g-C sample and for more ordered particles ED patterns are consistent with the hexagonal phase of the Ru metal, space group P63/mmc (Fig. 8c). The larger nanoparticles were predominantly (101) and (002) crystal orientations. Other loadings exhibited similar behaviour. Some of the larger particles of about 5 and 7 nm on the graphitic carbon support are shown in Fig. 8(e), which is an enlarged area from the Fig. 8(b).
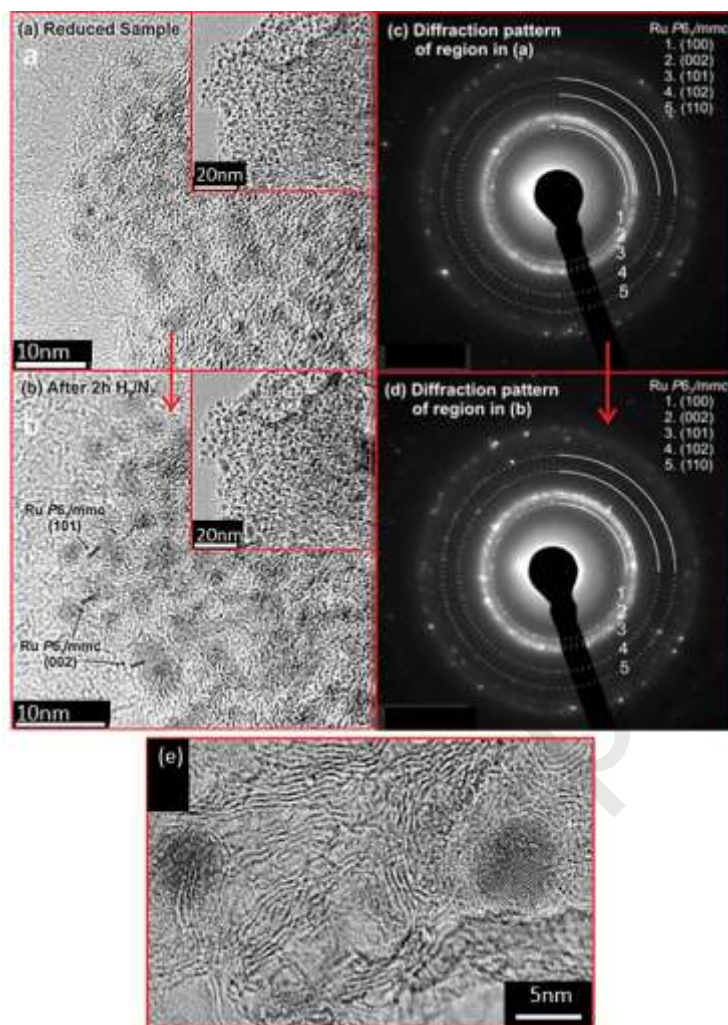
Fig. 8. Real time Dynamic ETEM experiments of Ru/g-C in controlled 3:1 H2/N2 mixture: top: (a) and (c) image and the corresponding electron diffraction after initial hydrogen reduction (post reduction sample); and bottom: (b) and (d) show the nanoparticle growth and dynamic electron diffraction following 2 hours in ammonia synthesis. (e) An enlarged area from (b), illustrating larger and therefore more widely spaced Ru nanoparticles of about 5 to 7 nm in size, on the graphitic carbon support in ammonia synthesis.

The Ru sample reveals a large number of Ru single atoms and clusters in addition to Ru nanoparticles. It is believed that active sites for N_2 dissociative adsorption is the rate determining step in ammonia synthesis [28,33]. Ru single atoms and Ru atom clusters observed in our dynamic studies may impact the N_2 adsorption properties in ammonia synthesis. Additionally, the Ru particles are observed to grow faster on graphitic supports.

The resulting shape changes can also affect the catalytic active sites on the Ru surfaces and the catalytic activity. Faster growth of Ru particles on graphitic carbon indicates higher mobility of the particles on the support.

Our observations of the dynamic growth of Pt nanoparticle (NP) catalysts on graphite in oxidation at higher temperatures (500 ℃) show that they grow faster indicating that the particles are more mobile. In reducing gases of H_2 and N_2 the Ru particles are also observed to grow faster on graphitic carbon supports at a similar temperature (of 450 ℃), consistent with Pt/graphite, irrespective of the gas environment.

4. Conclusions

In-situ visualization and analyses of Pt/graphite in controlled oxidation reactions as a function of temperature and of practical Ru nanocatalysts on graphtic carbon and carbon supports in ammonia synthesis have been carried out in real time, using ESTEM and ETEM with single atom resolution. The observations demonstrate atomic scale reaction dynamics and reveal the presence of single atoms and atom clusters, in addition to nanoparticles, which play a key role in the dispersion, mobility, growth and stability of the nanocatalysts. The effect of the graphite support on the size, mobility and stability of Pt nanocatalyst particles in oxidation as a function of operating temperatures is described. In supported Ru nanocatalysts, dynamic studies have revealed morphological changes with well-faceted Ru nanoparticles on the amorphous carbon support, whereas the nanoparticles on the graphitic carbon are generally irregular and include some larger particles. The findings provide a pathway to understand and control the size, agglomeration and stability of the nanoparticle catalysts, crucial to their production and applications. The single atom resolution-ESTEM

development opens up new opportunities to visualize and understand the dispersion and

stability of single atoms and small clusters on more complex supports.

Acknowledgments

The authors declare no competing financial interest.

References

[1]   S. Zhang, X Yuan, H. Wang, K. A. Friedrich, M. Schulze, J. Power Sour. 194 (2009) 588-598 (and references therein).

[2]   A. Russell, W.S. Epling, Catal. Rev. Sci. Eng. 53 (2011) 337-353.

[3]   E.D. Boyes, A.P. LaGrow, M.R. Ward, R.W. Mitchell, P.L. Gai, Accts. Chem. Res. 53 (2020) 390-399.

[4]   E.D. Boyes, P.L. Gai, Ultramicroscopy, 67 (1997) 219-232.

[5]   P.L. Gai, E.D. Boyes, Microsc. Res. Tech. 72 (2009)153-164.

[6]   P.L. Gai, Microsc. Microanal. 8 (2002) 21-28.

[7]   P.L. Gai, K. Kourtakis, E.D. Boyes, Catal. Lett. 102 (2005) 1-7.

[8]   M.R. Ward, T. Hyde, E.D. Boyes, P.L. Gai, ChemCatChem, 4 (2012) 1622-1631.

[9]   M.H. Shao, A. Peles, K. Shoemaker, Nano Letters, 11 (2011) 3714-3719.

[10] M. Chourashiya, S.T. Vindt, A.A.V. Palenzuel, C.M. Pedersen, C. Kallesøe, S.M. Andersen, International Journal of Hydrogen Energy, 43 (2018) 23275-23284.

[11] P. Wynblatt, N.A. Gjostein, Acta Metallurgica, 24 (1976) 1165-1174.

[12] T. Hansen, S.R. DeLaRiva, A. Challa, A. Datye, Acc. Chem. Res. 46 (2013) 1720-1730.

[13] B.T. Qiao, A. Wang, X. Yang, L. Allard, Z. Jiang, Y. Cui, T. Zhang, Nature Chem. 3 (2011) 634-641.

[14] S. Sun, Scientific Reports, 3 (2013) 1775-1777.

[15] X.Yang, A. Wang, B. Quiao, J. Li, J. Liu, T. Zhang,
      Accts. Chem. Res. 6 (2013) 1740-1748.

[16] F. Dvorak, M. Camellone, A. Andrii Tovt, N. Tran, F. Negreiros, M. Vorokhta , T.
      Ska´la , I. Matolınova, J. Myslivecˇek , V. Matolı, S. Stefano Fabris, Nature
      Comm. 7 (2016) 10801-10804.

[17] J.S. King, A. Wittstock, J. Biener, S.O. Kucheyev, Y.M. Wang, T.F. Baumann,
      S. Giri, A.V. Hamza, M. Baeumer, S.F. Bent, Nano Letters, 8 (2008) 2405-2409.

[18] S.B. Simonsen, I. Chorkendorff, S. Dahl, M. Skoglundh, J. Sehested, S. Helveg,
      J. Catal. 281 (2011) 147-155.

[19] A.V. Crewe, J. Wall, J. Langmore, Science, 168 (1974) 1338-1341.

[20] B. Zhang, W. Zhang, D.S. Su, ChemCatChem, 3 (2011) 965-968.

[21] M. Haider, S. Uhlemann, E. Schwan, H. Rose, B. Kabius, K. Urban, Nature 392 (1998)
      768-769.

[22] P.E. Batson, N. Delby, O. Krivanek, Nature, 418 (2002) 617-620.

[23] E.D. Boyes, M.R. Ward, L. Lari, P.L. Gai, Ann. Phys. (Berlin), 525 (2013) 423-429.

[24] E.D. Boyes, P.L. Gai, Comptes. Rendu. Phys. 15 (2014) 200-213.

[25] P.L. Gai, L. Lari, M.R. Ward, E.D. Boyes, Chem. Phys. Lett. 592 (2014) 355.

[26] E.D. Boyes, P.L. Gai, MRS Bull. 40 (2015), 600-604.

[27] L. Lloyd, Handbook of Industrial Catalysts, Springer, New York, 2011.

[28] D.E. Brown, T. Edmonds, R.W. Joyner, J.J. McCarroll, S.R. Tennison, Catal. Lett. 144
      (2014) 545-552.

[29] J. Okal, L. Kęnipiński, Catal. Lett. 128 (2009) 331-336.

[30] Z. Kowalczyk, S. Jodzis, J. Sentek, Appl. Catal. A, 138 (1996) 83-91.

[31] F. Rosowski, A. Hornung, O. Hinrichsen, D. Herein, M. Muhler, G. Ertl, Appl. Catal.
      A, 151 (1997) 443-460.

[32]   J. Wellenbüscher, M. Muhler, W. Mahdi, U. Sauerlandt, J. Schultze, G. Ertl, R.
       Schlögl, Catal. Lett. 25 (1994) 61-74.

[33] Z. Song, T. Cai, J. Hanson, J.A. Rodriguez, J. Hrbek, J. Am. Chem. Soc. 126 (2004)
      8576-8584.

[34] P.L. Gai, K. Kourtkis, Science. 267 (1995) 661-663.

[35] J. Haggin, Chem.Eng.News. 73 (1995) 39-41.

[36]   P.L. Gai, Adv. Materials, 10 (1998) 1259-1263.

[37] P.L. Gai, E.D. Boyes, P. Hansen, S. Helveg, S. Giorgio, C. Hentry, MRS Bull. 32
      (2007) 1044-1048.

[38] M. Jacoby, Chem. Eng, News. 80 (2002) 26-29.

[39] P.L. Gai, J. Montero, A. Lee, K. Wilson, E.D. Boyes, Catal.Lett. 132 (2009) 182-188.

[40] P.L. Gai, K. Yoshida, M.R. Ward, M. Walsh, R.T. Baker, L. van de Water,

M.J. Watson, E.D. Boyes, Catal. Sci. Technol. 6 (2016) 2214-2227.

[41] A.P. LaGrow, M.R. Ward, D.C. Lloyd, P.L.Gai, E.D. Boyes, J. Am. Chem. Soc. 139
       (2017) 179-185.

[42] M.R. Ward, B. Theobald, J. Sharman, E.D. Boyes, P.L. Gai, J. Microscopy. 269 (2018)
       143-150.

[43] R.W. Mitchell, D.C. Lloyd, L.G.A. van de Water, P.R. Ellis, K.A. Metcalfe,
       C. Sibbald, L.H. Davies, D.I. Enache, G.J. Kelly, E.D. Boyes, P.L. Gai,
       ACS Catalysis, 8 (2018) 8816-8829.

[44] M.J. Walsh, K. Yoshida, A. Kuwabara. M. Pay, P.L. Gai, E.D. Boyes, Nano Letters.
       12 (2012) 2027-2031.

[45] A. Scott, Chem.Eng.News. 91 (2013) 32.

[46] G. Somorjai, R. York, D. Butcher, J.Y. Park, Phys.Chem.Chem.Phys. 9 (2007) 3500-
       3513.

Graphical abstract